

# Bound states in doped charge transfer insulator

Pengfei Li,<sup>1,2</sup> Yang Shen,<sup>3</sup> Mingpu Qin,<sup>3</sup> Kun Jiang,<sup>1,2</sup> Jiangping Hu,<sup>1,2,4</sup> and Tao Xiang<sup>1,2</sup>

<sup>1</sup>Beijing National Laboratory for Condensed Matter Physics and Institute of Physics, Chinese Academy of Sciences, Beijing 100190, China

<sup>2</sup>School of Physical Sciences, University of Chinese Academy of Sciences, Beijing 100190, China

<sup>3</sup>Key Laboratory of Artificial Structures and Quantum Control (Ministry of Education),

School of Physics and Astronomy, Shanghai Jiao Tong University, Shanghai 200240, China

<sup>4</sup>New Cornerstone Science Laboratory, Beijing, 100190, China

(Dated: August 2, 2024)

Understanding the physics of doping a charge transfer insulator is the most important problem in high-temperature superconductivity. In this work, we show that an in-gap bound state emerges from the localized hole of the doped charge transfer insulator. We propose an approximate ground state wavefunction based on one localized Zhang-Rice singlet and the Neel state. By calculating the excitation states with one hole added and removed from this ground state, we successfully identify the existence of bound states inside the charge transfer gap. This feature is further proved by the MPS-based Lanczos study of a system of  $4 \times 4$  CuO<sub>2</sub> unit cells. How these bound states evolve into metallic states is further discussed. Our findings identify the key component of recent STM results on lightly doped Ca<sub>2</sub>CuO<sub>2</sub>Cl<sub>2</sub> and provide a new understanding of hole-doped charge transfer insulators.

As a relative of Mott insulator, the concept of charge transfer (CT) insulator plays an important role in the understanding of the insulating behaviors in correlated transition metal insulators, especially in cuprates [1, 2]. The key energy scale for charge transfer insulators is the charge-transfer energy between  $d$  electrons and their neighbor  $p$  electrons  $\Delta_{CT}$ , instead of the onsite Hubbard repulsion energy  $U$  for the  $d$  electrons. Therefore, the doped holes in cuprates reside primarily on oxygen sites and together with the hole in the Cu site. They form the well-known Zhang-Rice (ZR) singlets because the Cu<sup>3+</sup> ( $3d^8$ ) state has a higher energy [3]. These singlets are the dominant charge carriers in the hole-doped cuprates and become superconducting under the influence of super-exchange interaction  $JS_iS_j$  between  $d$  electrons of Cu [3]. Although this effective single-band  $t$ - $J$  model and the corresponding Hubbard model are extensively explored [4, 5] and the condition for the appearance of superconductivity is studied recently [6–8], a comprehensive understanding of the process of doping the charge transfer insulator and Mott insulator is a central theme for the ultimate understanding of the high-temperature superconductivity [9].

Recently, a new scanning tunneling microscopy (STM) experiment was carried out on the extremely lightly doped cuprates Ca<sub>2</sub>CuO<sub>2</sub>Cl<sub>2</sub> (CCOC) [10]. The Na<sup>1+</sup> atoms are introduced to replace Ca<sup>2+</sup> atoms resulting in hole doping. Surprisingly, bound states inside the charge transfer gap of CCOC were observed, as illustrated in Fig.1(a) [10]. The spatial tunneling spectrum distribution for these bound states shows a similar contour of the Zhang-Rice singlet. This new observation provides great opportunity to understand the hole-doped charge-transfer insulators and Mott insulators [11–15]. In this work, we provide a comprehensive study of the doped charge transfer insulator and point out the bound states are indeed related to the localized Zhang-Rice singlets.

There are two important energy scales for the above observations, the CT gap  $\Delta_{CT} \approx 2eV$  and the bound state energy  $E_b \approx 0.6 - 0.7eV$ . These two energy scales are much larger

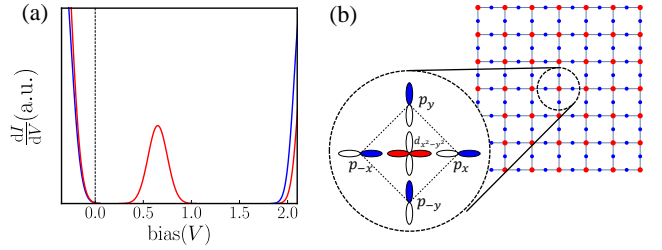


FIG. 1. (a) The schematic scanning tunneling spectroscopy density of states in lightly Na doped cuprates Ca<sub>2</sub>CuO<sub>2</sub>Cl<sub>2</sub> [10]. The red line is the spectrum away from the Na-doped center while the blue line is the spectrum at the Na-doped center. A bound state around  $E_b \approx 0.6 - 0.7eV$  shows up at the charge transfer gap. (b) The essential CuO<sub>2</sub> lattice of cuprates superconductors. Around each Cu, there are four neighbor oxygens. The most relevant orbitals are Cu  $3d_{x^2-y^2}$ , O  $2p_x$  and O  $2p_y$ , as illustrated in the inset.

than the exchange energy  $J \sim 0.14eV$  and the hopping scale  $t \sim 0.35eV$  [16]. Hence, the kinetic energy and exchange energy can be treated as perturbations for the bound states in a doped CT insulator. This is the central starting point for our following discussions. Another important fact is that the bound states observed in STM experiment [10] are localized, or more precisely, *the ZR singlets are localized*. In the following discussion, we will show that the appearance of in-gap bound states results from the localized ZR singlet state.

With these two facts, we start from a qualitative perspective and propose the below classical product state wavefunction  $|GS\rangle$  as the approximated ground state wavefunction, which provides a qualitative description of the hole-doped CT insulator in the background of antiferromagnetism (AFM):

$$|GS\rangle = \psi_{0A}^\dagger d_{0A\uparrow} |AFM\rangle. \quad (1)$$

Following the conventional notation [3], we define the vacuum  $|\nu a\rangle$  as the fully filled Cu  $d^{10}$  and O  $p^6$  states from the

hole picture.  $d_{i\alpha\sigma}^\dagger$  is the hole creation operator for Cu  $3d_{x^2-y^2}$  at unit cell  $i$  and AFM sublattice index  $\alpha = A, B$ .  $|AFM\rangle$  is the Neel AFM wavefunction. The  $\psi_{0A}^\dagger$  is the ZR singlet operator for the bound site at center 0 and sublattice A. The exact form of  $\psi_{0A}^\dagger$  will be discussed below as an extension of the ZR singlet proposed in the original Zhang-Rice paper [3]. We also assume there are total  $N$  holes for the ground states. More precisely, there is one hole for each magnetic site and two holes for the ZR site.

Indeed, the AFM Neel state should not be the ground state for the Heisenberg model and the half-filled Hubbard model owing to the quantum fluctuations in two dimensions [17]. However, the energy difference between the Neel state and the true ground state should be less than order  $J$ . Then, we can safely argue the Neel state is enough for the localized bound state problem. On the other hand,  $\psi_{0A}^\dagger$  may also deviate from the exact state, which is also a controllable perturbation. Therefore,  $|GS\rangle$  is a faithful approximate ground state.

Before a more detailed discussion, we introduce the three-band Hamiltonian [3, 18] below

$$\begin{aligned}
H = & \tilde{\epsilon}_d \sum_i d_{i\sigma}^\dagger d_{i\sigma} + \tilde{\epsilon}_p \sum_l p_{l\sigma}^\dagger p_{l\sigma} + U \sum_i \hat{n}_{d\uparrow} \hat{n}_{d\downarrow} \\
& + \sum_{\langle il \rangle} t_{pd} (d_{i\sigma}^\dagger p_{l\sigma} + h.c.) - \sum_{\langle ll' \rangle} t_{pp} (p_{l\sigma}^\dagger p_{l'\sigma} + h.c.) \\
& + E_{loc} \sum_\delta P_{0\delta\sigma}^\dagger P_{0\delta\sigma}
\end{aligned} \quad (2)$$

where  $p_{l\sigma}^\dagger$  is the hole creation operator for O ( $2p_x, 2p_y$ ) at site  $l$ .  $t_{pd}$  and  $t_{pp}$  are hopping integrals involving  $p-d$  and  $p-p$  processes respectively.  $\tilde{\epsilon}_{d/p}$  is the on-site potential for  $d/p$  orbitals in the hole picture respectively. More importantly, we add a  $E_{loc}$  term for the local potential energy at O atoms around the bound site due to dopants, which stabilize a localized ZR solution. The strong coupling theory of the three-band model without hole doping is the Heisenberg model. Moving to the hole doping, the three-band Hamiltonian becomes the standard  $t$ - $J$  model as discussed by Zhang and Rice [3].

Since we focus on the tunneling spectrum of STM, the tunneling density of states (DOS) at voltage  $V$  at  $\mathbf{r}$  following Fermi's golden rule can be written as

$$\begin{aligned}
\frac{dI}{dV}(\mathbf{r}, \omega) \propto & \sum_n |\langle n | \phi_\sigma^\dagger(\mathbf{r}) | GS \rangle|^2 \delta(-\omega - E_n + E_{GS}) \\
& + \sum_m |\langle m | \phi_\sigma(\mathbf{r}) | GS \rangle|^2 \delta(-\omega - E_{GS} + E_m)
\end{aligned} \quad (3)$$

where  $\phi_\sigma^\dagger(\mathbf{r})$  will be equal to  $d_{i\sigma}^\dagger$  or  $p_{l\sigma}^\dagger$  depending on the position and  $\omega$  is the energy in the unit of  $eV$ .  $|n\rangle$  are adding hole excitation eigenstates with hole number  $n > N$  and  $|m\rangle$  are removing hole excitation eigenstates with hole number  $m < N$ . Note that we have switched the energy  $\omega$  in the delta functions to the electron picture for experimental comparison. Hence, the gap for the insulating behavior is related to

$$\Delta_{gap} = E_{N+1} + E_{N-1} - 2E_{GS} \quad (4)$$

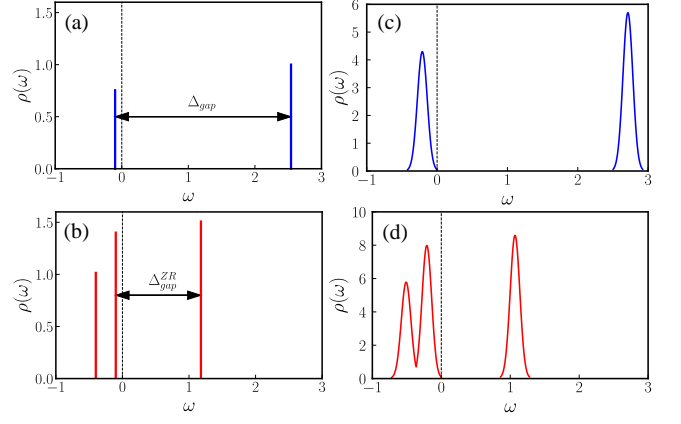


FIG. 2. (a),(b) The tunneling DOS  $\rho(\omega)$  calculated away from the ZR center and at the ZR center of ground state  $|GS\rangle$  respectively. The three-band parameters we used here are adapted from an ab initio calculation for CCOC with  $t_{pd} = 0.78eV$ ,  $t_{pp} = 0.15eV$ ,  $\tilde{\epsilon}_p - \tilde{\epsilon}_d = 3.25eV$ ,  $U = 9.5eV$  [23]. We add the local potential  $E_{loc} = -2t_{pd}$  on O atoms. (c),(d) The schematic broadening tunneling DOS of (a),(b) taking other effects into account, especially the motion effect.

Now, we can apply the above formulas to our case. Firstly, we focus on the spectrum away from the ZR center. The tunneling process is just equivalent to the AFM tunneling spectrum. For the  $|n\rangle$  excitation with  $N+1$  holes, the problem is reduced to a single hole moving in the background of the quantum antiferromagnet [19, 20]. As discussed above,  $t$  and  $J$  are perturbations. We can use the *local eigenstates* as the approximated states for the spectrum problem. For example, we use the localized ZR singlet to replace the moving hole as the approximation excited state  $|n\rangle$  [21]. Hence, the spectrum problem reduces to exact diagonalization problems around one Cu cell as illustrated in Fig.1 (b) [22]. Using the local  $D_4$  symmetry, we can group the four  $p$  orbital into one  $b_1$ , one  $a_1$  and two degenerate  $e$  symmetric basis:

$$\begin{aligned}
b_\sigma &= (p_{x\sigma} - p_{y\sigma} - p_{-x\sigma} + p_{-y\sigma})/2 \\
a_\sigma &= (p_{x\sigma} + p_{y\sigma} - p_{-x\sigma} - p_{-y\sigma})/2 \\
e_{1\sigma} &= (p_{x\sigma} + p_{-x\sigma})/\sqrt{2}, e_{2\sigma} = (p_{y\sigma} + p_{-y\sigma})/\sqrt{2}
\end{aligned} \quad (5)$$

Their corresponding energies become  $\epsilon_b = \tilde{\epsilon}_p - 2t_{pp}$ ,  $\epsilon_a = \tilde{\epsilon}_p + 2t_{pp}$  and  $\epsilon_e = \tilde{\epsilon}_p$ . Due to  $d_\sigma$  only has  $b_1$  symmetry, it only has overlap with  $b_\sigma$  orbital.

Locally, the local ground state  $|\psi_{1h}\rangle$  with one hole filling is the slight mixing between  $|d_\uparrow\rangle$  and  $|b_\uparrow\rangle$ . Here, we choose one spin-up polarized state without loss of generality. The lowest energy two-hole state  $|\psi\rangle$  is the mixing between ZR singlet  $(|d_\uparrow b_\downarrow\rangle - |d_\downarrow b_\uparrow\rangle)/\sqrt{2}$ ,  $|d_\uparrow d_\downarrow\rangle$  and  $|b_\uparrow b_\downarrow\rangle$ . With these states, we can directly calculate the spectrum as plotted in Fig.2(a). The gap  $\Delta_{gap}$  between  $N \rightarrow N-1$  ( $\omega > 0$ ) and  $N \rightarrow N+1$  ( $\omega < 0$ ) is around  $2.8eV$  owing to the charge transfer process.

Next, we move to the localized ZR center. We can also calculate the tunneling spectrum as shown in Fig.2(b). Now, the gap  $\Delta_{gap}^{ZR}$  at the ZR center has reduced to  $1.2eV$ . There is

indeed an in-gap bound state inside the charge transfer  $\Delta_{gap}$ . The essential reason for this bound state is owing to the fact that the local ground state wavefunction has changed to the localized ZR state as defined in Eq. 1. Hence, the removing hole process ( $N \rightarrow N-1$ ) is between ZR  $|\psi\rangle$  and  $|\psi_{1h}\rangle$ . Adding hole process ( $N \rightarrow N+1$ ) is between ZR  $|\psi\rangle$  and a three-hole excitation state  $|\psi_{3h}\rangle$ . There are two degenerate lowest energy three-hole excitation states  $|\psi_{3h}\rangle = e_{1\sigma}^\dagger|\psi\rangle$  and  $|\psi_{3h}\rangle = e_{2\sigma}^\dagger|\psi\rangle$ . Hence,  $\Delta_{gap}^{ZR}$  is reduced to new 1.2eV bound state. Besides these two states,  $|\psi_{3h}\rangle$  can also be other combinations leading to other peaks at lower energy.

Clearly, the above bound state result depends on the parameters we choose. Here, we adopt the realistic parameter based on a combined local density functional theory (DFT-LDA) and quantum Monte Carlo work for doped cuprates and CCOC [23]. We also test the other parameters used in Ref. [22] and [21]. Similar bound states show up, although the actual gap sizes vary in different cases. Additionally, we also need to consider the motion effect of a single hole or a single electron in the background of quantum antiferromagnetic. Historically, this hole motion has been investigated by a self-consistent perturbation theory and other methods [19–21, 24–26]. The resulting bandwidth  $W_h$  is about  $2 \sim 3 J$ . The bandwidth  $W_e$  is also around the same order [21]. Hence, the energy level we discussed above should be further broadened to  $W_h$  or  $W_e$ , as illustrated in Fig.2(c) and Fig.2(d).

After gaining a qualitative understanding, we want to provide more evidence from many-body computation. We employ the MPS-based Lanczos method for the calculation of the spectrum function [27]. The strategy is to represent the Lanczos basis in the matrix-product state (MPS). A special reorthogonalization process is performed after the standard Lanczos method to resolve the loss of orthogonality resulting from the compression of MPS [27]. The spectrum functions are then obtained from the eigenstates obtained by Lehmann representation [27].

The system we studied consists of  $4 \times 4$  CuO<sub>2</sub> unit cells (shown in the inset of Fig. 3). Since the ZR singlet state is localized in our setup as discussed above, the finite size effect should be small and the  $4 \times 4$  system is enough for the main feature. The bond dimension for MPS in the calculation is 2000 and the results remain almost unchanged with larger bond dimensions. We add the localization potential to the 4  $p$  orbitals surrounding a Cu  $d$  orbital (the dashed circle in the inset of Fig. 3). A magnetic pinning field with strength  $h_m = 0.5$  is also applied to the Cu site in the downright corner to show the spin pattern in the system. The distribution of holes and local spin for the one hole-doped system can be found in the inset in Fig. 3, where we find the doped hole is indeed pinned to the desired oxygen sites forming a localized ZR with the hole in the center Cu site.

The local DOS at the same Cu site for the half-filling and one-hole doped systems are plotted in Fig. 3. We distinguish the local DOS of adding electron and hole processes with filled and open markers. For the blue square lines, the tunneling process is for the half-filling CT insulator. We obtain a

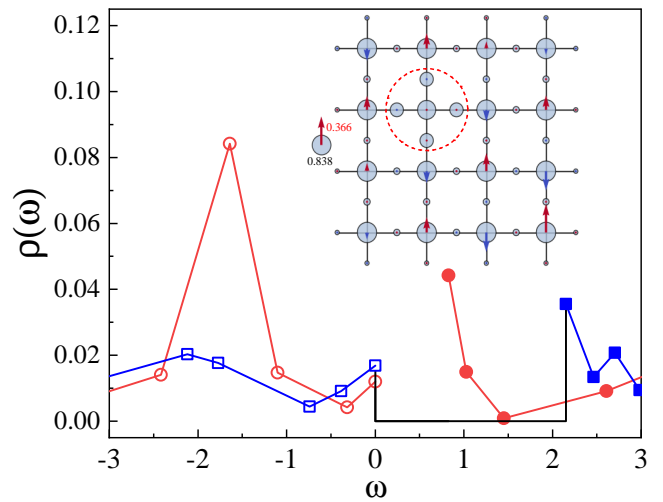


FIG. 3. Local DOS  $\rho(\omega)$  for a system consisted of  $4 \times 4$  CuO<sub>2</sub> unit cells from MPS-based Lanczos method. Only lower energy results are plotted here and the broader energy range results can be found in the supplementary materials. The blue and red lines represent results for half-filled and one extra hole-doped systems respectively. The filled (open) markers represent result for processes adding one electron (hole). The  $\Delta_{gap}$  for CT is highlighted by the black line. In the inset, we plot the spin and hole distribution for the ground state with one extra hole doping, where we can see the doped holes mainly reside on the four oxygen sites (in the dashed circle) with local energy decreased. A magnetic pinning field is also applied in the Cu site in the downright corner to show the spin pattern in the system. The radius (length) of circles (arrows) is proportional to the hole (spin) density and the direction of the arrow means the sign of the spin density. The legend in the inset shows a site with hole density 0.838 and spin density 0.366.

charge transfer gap of about 2.15 eV (highlighted by the black line), which is improved closer to the experimental value than 2.8 eV in Fig.2. More importantly, from the result of the one-hole doped case as shown in the red circle line, we can find a finite density of states inside the charge transfer gap. This newly emerged bound state matches well with our qualitative discussion, proving the existence of localized ZR. The new gap  $\Delta_{gap}^{ZR}$  is about 0.8 eV, which is consistent with the experimental observations [10].

For the understanding of STM measurement, we also need to take the tunneling matrix effect into account [28, 29]. STM tip coupling with the CCOC mainly through the top Cl  $p_z$  orbitals as shown in Fig.4(a). Cl atoms directly sit above the Cu sites. The overlap between  $p_z$  and  $d_{x^2-y^2}$  directly beneath it is strictly zero by symmetry. However,  $p_z$  has overlap with  $p_{x(y)}$  of O atom and through the overlap  $p_z$  state hybridizes with the hole state centered on the nearest neighbor (NN) Cu atom. Hence, the operator  $\phi_{\sigma}^{\dagger}(\mathbf{r})$  in Eq.3 should be modified to

$$\phi_{\sigma}^{\dagger}(\mathbf{r}) = \sum_{\tau} (-1)^{P_{\tau}} \langle \mathbf{r}|i, Cl \rangle p_{i,\tau,\sigma}^{\dagger} + \sum_{\tau} (-1)^{D_{\tau}} \langle \mathbf{r}|i, Cl \rangle d_{i+\tau,\sigma}^{\dagger} \quad (6)$$

where  $\langle \mathbf{r}|i, Cl \rangle$  is the overlap between STM tip and Cl  $p_z$  state at site  $i$ . The first term describes the tunneling to O  $p_{x(y)}$

around the Cu at site  $i$  in which  $(-1)^{P_\tau} = -1$  for  $\tau = -x, -y$  and  $(-1)^{P_\tau} = 1$  for  $\tau = x, y$  according to symmetry. The second term describes the tunneling to NN Cu  $d_{x^2-y^2}$  through O in which  $(-1)^{D_\tau} = -1$  for  $\tau = \pm x$  and  $(-1)^{D_\tau} = 1$  for  $\tau = \pm y$ .

Fig.4(b) shows the DOS map if STM scans the sample at the energy of in-gap bound state. When the STM tip is placed at the position of the ZR center, it couples with  $a_1$  state of the four O atoms around it due to the factor in the first term of Eq.6. However, the in-gap state spectrum has no contribution of O  $a_1$  state and NN Cu in the previous calculation. Thus the DOS signal vanishes at the ZR center. Whereas at the position of NN Cu, STM tip can couple to one O  $p_{x(y)}$  and Cu  $d_{x^2-y^2}$  of the ZR cell, which has spectral weight at in-gap state energy. Thus, STM maps the DOS at NN Cu of the ZR center, which is qualitatively consistent with the experiment observed ZR-like contour [10].

Finally, a natural question arising from the in-gap bound states is how these bound states evolve into metallic states. A straightforward calculation is challenging owing to the complicated spin pattern and random doping. There is one way to determine the critical hole doping density  $x_c$  by comparing  $E_b$  and the coherent hole motion bandwidth. We use the renormalized mean field of  $t$ - $J$  model based on Gutzwiller approximation to estimate bandwidth  $W_{GW}$  [30, 31]. The hopping renormalization factor is  $g_t = \frac{2x}{1+x}$  while the spin exchange renormalization factor is  $g_s = \frac{4}{(1+x)^2}$ .  $x$  is the average hole doping density  $1 - \langle \hat{n} \rangle$ . By decoupling the  $JS_iS_j$  into the nearest neighbor hopping bond, we find the  $W_{GW}$  of renormalized  $t$ - $J$  model is about  $0.65eV$  at  $x = 0.046$ . Hence, the  $x_c$  is estimated around 5%. This estimation is consistent with experimental findings in Na-doped CCOC [32–34], where superconductivity only emerges after  $x > 5\%$ . Hence, if the charge-transfer insulator is undoped, a charge-transfer gap  $\Delta_{gap}$  dominates the charge dynamics of the antiferromagnetic insulating ground state, as illustrated in Fig.4(c). Then, keeping light-doping the system, a bound state with the tunneling gap  $\Delta_{gap}^{ZR}$  emerges from the charge-transfer gap as illustrated in Fig.4(e), where ZR singlets are randomly localized. If the kinetic energy overcomes the binding energy, an itinerant ZR band overlaps with the valence band showing a metallic behavior as illustrated in Fig.4(f).

In summary, we successfully identify the origin of the in-gap bound states emerged from the lightly doped charge transfer insulator using an approximate ground-state wavefunction based on one localized Zhang-Rice singlet and the Neel state. By calculating the tunneling spectrum, the tunneling gap  $\Delta_{gap}^{ZR}$  at the ZR center is around half of the charge-transfer gap  $\Delta_{gap}$ . Moreover, we carry out MPS-based Lanczos calculations on system consisted of  $4 \times 4$  CuO<sub>2</sub> unit cells with local potential to pin the Zhang-Rice singlet. The results show a bound state with 0.8 eV emerges within the charge transfer gap. Taking the STM tunneling matrix effect into account, the tunneling contour at the bounding energy around the ZR center is weak while the four neighbors are strong. How these bound states evolve into metallic states is further discussed. All these findings are consistent with the recent experiment observations in

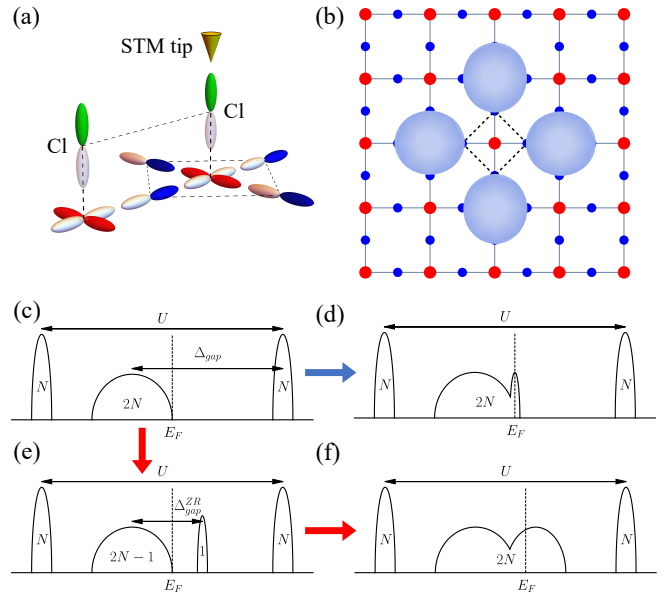


FIG. 4. (a) Schematic diagram of the STM tip coupling to CCOC through  $p_z$  orbitals of Cl directly above Cu  $d_{x^2-y^2}$ . (b) Schematic STM tunneling contour of the electronic state on the CuO<sub>2</sub> lattice. The dashed box indicates the ZR state. In our calculation, we only have tunneling DOS at Cl lattice sites without considering the atomic wavefunctions. (c-f) Schematic diagram of the two different scenarios of insulator-metal transition process  $c \rightarrow d$  and  $c \rightarrow e \rightarrow f$ . (c) For the undoped CT insulator, the system is in an antiferromagnetic insulating state with a charge transfer gap. (d) In the first scenario, the doped holes emerge from the O 2p band and no in-gap states occur. (e) In the second scenario, when the system is lightly hole doped, the doped holes form localized ZR bound states emerging in the gap, and the system remains in an insulating state. (f) As the doping concentration increases, the in-gap ZR bound states begin to overlap, forming a ZR band that touches the valence band, leading to a transition to a metallic state.

lightly hole-doped CCOC [10] and provide a comprehensive understanding of doped charge-transfer insulators.

*Acknowledgement:* We thank Yayu Wang and Shusen Ye for helpful discussion of their experimental results. We acknowledge the support by the Ministry of Science and Technology (Grant No. 2022YFA1403900), the National Natural Science Foundation of China (Grant No. NSFC-11888101, No. NSFC-12174428, No. NSFC-11920101005 and No. NSFC-12274290), the New Cornerstone Investigator Program, and the Chinese Academy of Sciences Project for Young Scientists in Basic Research (2022YSBR-048).

- 
- [1] J. Zaanen, G. A. Sawatzky, and J. W. Allen, Band gaps and electronic structure of transition-metal compounds, *Phys. Rev. Lett.* **55**, 418 (1985).
  - [2] D. Khomskii, *Transition Metal Compounds* (Cambridge University Press, 2014).

- [3] F. C. Zhang and T. M. Rice, Effective hamiltonian for the superconducting Cu oxides, *Phys. Rev. B* **37**, 3759 (1988).
- [4] S. Jiang, D. J. Scalapino, and S. R. White, Ground-state phase diagram of the  $t$ - $t'$ - $J$  model, *Proceedings of the National Academy of Sciences* **118**, e2109978118 (2021).
- [5] M. Qin, C.-M. Chung, H. Shi, E. Vitali, C. Hubig, U. Schollwöck, S. R. White, and S. Zhang (Simons Collaboration on the Many-Electron Problem), Absence of superconductivity in the pure two-dimensional hubbard model, *Phys. Rev. X* **10**, 031016 (2020).
- [6] H. Xu, C.-M. Chung, M. Qin, U. Schollwöck, S. R. White, and S. Zhang, Coexistence of superconductivity with partially filled stripes in the hubbard model, *Science* **384**, eadh7691 (2024), <https://www.science.org/doi/pdf/10.1126/science.adh7691>.
- [7] X. Lu, F. Chen, W. Zhu, D. N. Sheng, and S.-S. Gong, Emergent superconductivity and competing charge orders in hole-doped square-lattice  $t$ - $j$  model, *Phys. Rev. Lett.* **132**, 066002 (2024).
- [8] H.-C. Jiang and S. A. Kivelson, High temperature superconductivity in a lightly doped quantum spin liquid, *Phys. Rev. Lett.* **127**, 097002 (2021).
- [9] P. A. Lee, N. Nagaosa, and X.-G. Wen, Doping a mott insulator: Physics of high-temperature superconductivity, *Rev. Mod. Phys.* **78**, 17 (2006).
- [10] S. Ye, J. Zhao, Z. Yao, S. Chen, Z. Dong, X. Li, L. Shi, Q. Liu, C. Jin, and Y. Wang, Visualizing the Zhang-Rice singlet, molecular orbitals and pair formation in cuprate (2023), [arXiv:2309.09260 \[cond-mat.supr-con\]](https://arxiv.org/abs/2309.09260).
- [11] H. Eskes, M. B. J. Meinders, and G. A. Sawatzky, Anomalous transfer of spectral weight in doped strongly correlated systems, *Phys. Rev. Lett.* **67**, 1035 (1991).
- [12] M. B. J. Meinders, H. Eskes, and G. A. Sawatzky, Spectral-weight transfer: Breakdown of low-energy-scale sum rules in correlated systems, *Phys. Rev. B* **48**, 3916 (1993).
- [13] E. Dagotto, Correlated electrons in high-temperature superconductors, *Rev. Mod. Phys.* **66**, 763 (1994).
- [14] A. Damascelli, Z. Hussain, and Z.-X. Shen, Angle-resolved photoemission studies of the cuprate superconductors, *Rev. Mod. Phys.* **75**, 473 (2003).
- [15] P. Phillips, Colloquium: Identifying the propagating charge modes in doped mott insulators, *Rev. Mod. Phys.* **82**, 1719 (2010).
- [16] C. Kim, P. J. White, Z.-X. Shen, T. Tohyama, Y. Shibata, S. Maekawa, B. O. Wells, Y. J. Kim, R. J. Birgeneau, and M. A. Kastner, Systematics of the photoemission spectral function of cuprates: Insulators and hole- and electron-doped superconductors, *Phys. Rev. Lett.* **80**, 4245 (1998).
- [17] P. W. Anderson, An approximate quantum theory of the antiferromagnetic ground state, *Phys. Rev.* **86**, 694 (1952).
- [18] V. J. Emery, Theory of high- $T_c$  superconductivity in oxides, *Phys. Rev. Lett.* **58**, 2794 (1987).
- [19] S. Schmitt-Rink, C. M. Varma, and A. E. Ruckenstein, Spectral function of holes in a quantum antiferromagnet, *Phys. Rev. Lett.* **60**, 2793 (1988).
- [20] C. L. Kane, P. A. Lee, and N. Read, Motion of a single hole in a quantum antiferromagnet, *Phys. Rev. B* **39**, 6880 (1989).
- [21] V. I. Belinicher, A. L. Chernyshev, and L. V. Popovich, Range of the  $t$ - $J$  model parameters for  $\text{CuO}_2$  planes: Experimental data constraints, *Phys. Rev. B* **50**, 13768 (1994).
- [22] J. H. Jefferson, H. Eskes, and L. F. Feiner, Derivation of a single-band model for  $\text{CuO}_2$  planes by a cell-perturbation method, *Phys. Rev. B* **45**, 7959 (1992).
- [23] P. R. C. Kent, T. Saha-Dasgupta, O. Jepsen, O. K. Andersen, A. Macridin, T. A. Maier, M. Jarrell, and T. C. Schulthess, Combined density functional and dynamical cluster quantum monte carlo calculations of the three-band hubbard model for hole-doped cuprate superconductors, *Phys. Rev. B* **78**, 035132 (2008).
- [24] S. Sachdev, Hole motion in a quantum Néel state, *Phys. Rev. B* **39**, 12232 (1989).
- [25] Z. B. Su, Y. M. Li, W. Y. Lai, and L. Yu, Self-consistent renormalized hole motion in a quantum antiferromagnet, *Phys. Rev. Lett.* **63**, 1318 (1989).
- [26] V. Y. Yushankhai, V. S. Oudovenko, and R. Hayn, Proper reduction scheme to an extended  $t$ - $J$  model and the hole dispersion in  $\text{Sr}_2\text{CuO}_2\text{Cl}_2$ , *Phys. Rev. B* **55**, 15562 (1997).
- [27] P. E. Dargel, A. Wöllert, A. Honecker, I. P. McCulloch, U. Schollwöck, and T. Pruschke, Lanczos algorithm with matrix product states for dynamical correlation functions, *Phys. Rev. B* **85**, 205119 (2012).
- [28] T. M. Rice and H. Tsunetsugu, A simple model for the checkerboard pattern of modulated hole densities in underdoped cuprates, *The European Physical Journal B - Condensed Matter and Complex Systems* **49**, 1 (2006).
- [29] Y. Chen, T. M. Rice, and F. C. Zhang, Rotational symmetry breaking in the ground state of sodium-doped cuprate superconductors, *Phys. Rev. Lett.* **97**, 237004 (2006).
- [30] F. C. Zhang, C. Gros, T. M. Rice, and H. Shiba, A renormalised hamiltonian approach to a resonant valence bond wavefunction, *Superconductor Science and Technology* **1**, 36 (1988).
- [31] P. W. Anderson, P. A. Lee, M. Randeria, T. M. Rice, N. Trivedi, and F. C. Zhang, The physics behind high-temperature superconducting cuprates: the ‘plain vanilla’ version of RVB, *Journal of Physics: Condensed Matter* **16**, R755 (2004).
- [32] Z. Hiroi, N. Kobayashi, and M. Takano, Probable hole-doped superconductivity without apical oxygens in  $(\text{Ca}, \text{Na})_2\text{CuO}_2\text{Cl}_2$ , *Nature* **371**, 139 (1994).
- [33] Y. Kohsaka, M. Azuma, I. Yamada, T. Sasagawa, T. Hanaguri, M. Takano, and H. Takagi, Growth of na-doped  $\text{Ca}_2\text{CuO}_2\text{Cl}_2$  single crystals under high pressures of several gpa, *Journal of the American Chemical Society*, *Journal of the American Chemical Society* **124**, 12275 (2002).
- [34] K. Waku, T. Katsufuji, Y. Kohsaka, T. Sasagawa, H. Takagi, H. Kishida, H. Okamoto, M. Azuma, and M. Takano, Charge dynamics of  $\text{Ca}_{2-x}\text{Na}_x\text{CuO}_2\text{Cl}_2$  as a correlated electron system with the ideal tetragonal lattice, *Phys. Rev. B* **70**, 134501 (2004).

## Supplemental Material: Bound states in doped charge transfer insulator

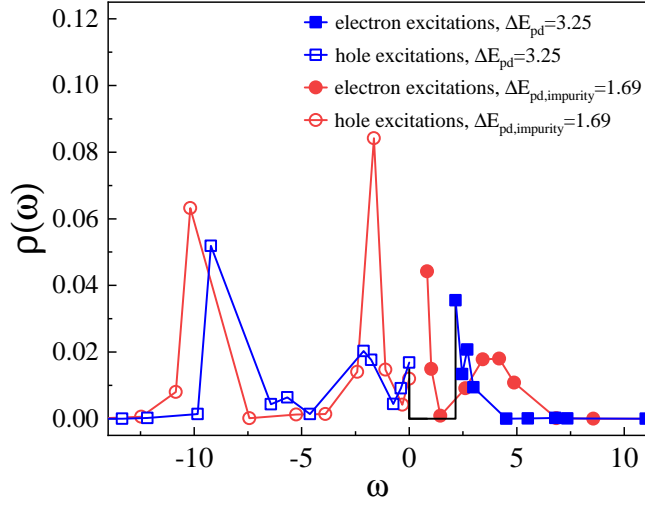


FIG. S1. LDOS for the same system in Fig. 3 in the main text (consisted of  $4 \times 4$   $\text{CuO}_2$  unit cells) from MPS-based Lanczos method. Here the energy range is broader than that in Fig. 3.

### LDOS for broader energy range for the $4 \times 4$ system

In Fig. S1, we show the LDOS result for the same system as in Fig. 3 in the main text (consisted of  $4 \times 4$   $\text{CuO}_2$  unit cells) from MPS-based Lanczos method. In Fig. 3 in the main text, results between  $-3$  eV and  $3$  eV are shown, while in Fig. S1, the LDOS for broader energy range is plotted, where we can identify the lower (around  $-9$  eV) and upper (around  $4$  eV) Hubbard bands.